Developed Heat Transfer Fluid Containing Nanoparticles

Reda I. Afify[1] S.F. Mansour[2], Khairy F. Megalaa[3], and M. Saad Mostafa[4]

[1]Faculty of Engineering at Shoubra, Mech. Department, Benha University, Cairo, Egypt.
[2]Faculty of Science at Zagazig, Zagazig University, Elsharqia, Egypt.
[3]Faculty of Engineering at El Mataria, Mech. Department, Helwan University, Cairo, Egypt.
[4] Higher Technological Institute, Tenth of Ramadan city, Egypt.
Eng.muhammad.saad@gmail.com

Abstract: The monitoring increase of world population and living standards accomplished with the massive demand of limited fossil fuel and dangerous nuclear fission emphasizes the global energy crisis. Solar power offers a viable option for solving the uprising energy crisis. Furthermore, there is a strong motivation to explore the possibility of harnessing solar thermal energy around the world, especially in locations with relatively high temperature (i.e Egypt). In the present work, the enhancement of both of thermal energy transfer and storage in a concentrated solar power (CSP) system was developed. The enhancement criteria stand on improving the thermal properties of the base fluid by adding nanoparticles (i.e alumina). Innovative eutectic halide salt (used in the current work) was chosen as a base heat transfer fluid for three main aspects which are i.) relatively high heat capacity, ii) wide working temperature range up to 850^{o}C, and iii) low cost compared to similar solutions. The Alumina (Al_2O_3) nanoparticles (prepared by citrate nitrate auto combustion technique "Pechini method") with 0.5%, 1%, 1.5%, 2% concentrations by weight were mixed with ternary halide eutectic salt composed of 13.4 wt.% NaCl, 33.7 wt.% KCl and 52.9 wt.% $ZnCl_2$ by the aid of a magnetic stirrer. The thermal properties of pure eutectic halide salt were investigated before and after adding nanoparticles (nanofluid). The main concerned parameters are the specific heat capacity, melting point, phase change temperature difference, heat of fusion and weight stability percentage. The experimental results show that specific heat capacity of the nanocomposites increased by increasing nanoparticle concentration. The observed enhancement in specific heat capacity was found to be 1.0416, 1.095, 1.196, 1.109 and 1.115 (J/g.^{o}C) respectively for various concentrations of 0.0%, 0.5 wt.%, 1.0 wt.%, 1.5 wt.% and 2.0 wt.% respectively. Consequently, the heat of fusion was to be 96.34, 71.64, 76.923, 71.98 and 70.67 for concentrations 0.0%, 0. 5 wt.%, 1.0 wt.%, 1.5 wt.% and 2.0 wt.% respectively. While, the stability of nanocompositions in liquid phase increased by increasing the concentrations of NPs.
[Reda I. Afify S.F. Mansour, Khairy F. Megalaa, and M. Saad Mostaf. **Developed Heat Transfer Fluid Containing Nanoparticles.** *Nat Sci* 2019;17(5):132-142]. ISSN 1545-0740 (print); ISSN 2375-7167 (online). http://www.sciencepub.net/nature. 16. doi:10.7537/marsnsj170519.16.

Key words: Concentrated solar power (CSP)**,** Renewable Energy (RE), Alumina (Al_2O_3) Nanoparticles, Eutectic halide salt, Pechini method).

1. Introduction and literature review

One of the most important issues faced people since the beginning of building civilizations was energy. Therefore, people were looking for easy ways to meet their energy needs. It could either be as simple as fire or be a coal-fired power plant to produce electricity to meet the same demands. According to International Energy Agency's (IEA) 2008 reported that fuel was the most used primary energy source with 33.1% and it was followed by coal with 27.0% and natural gas with 21.1%**[Uckun, 2013].**

Although the three different primary energy sources coal, oil and natural gases were used widely throughout the world to meet people's energy demands, all three energy sources have two common negative impacts on the world; air pollution and global warming. Especially low quality coal characterized by a lower heating value produced many harmful gases like Sulfur dioxide, Sulfur trioxide and Sulfuric acid (SO_2, SO_3 and H_2SO_4), respectively. Oil also produced harmful gases. Natural gas was cleaner than oil and coal, but it has also harmful effects on environment, including climate change. The burning of fossil fuels is considered, such as coal, oil and natural gases as an energy source isn't that much appropriate due to the release of greenhouse gases and other pollutants into the atmosphere that have negative impact to the earth. Also the stock of these fuels is undependable and is almost fading out by the year 2050. Figure (1) shows the previous recent and predicted amount of oil and gas liquid for varies regions of the earth.

According to the expected increase in population and the low production of fossil fuels (as it is depleted) over time, and pollution of the environment resulting from its operation, therefore, the renewable energy is considered an alternative solution to overcome this problem. Finally, it is known that the

solar energy represents the optimum choice for energy shortage (especially in Egypt) due to sunlight continues all the day.

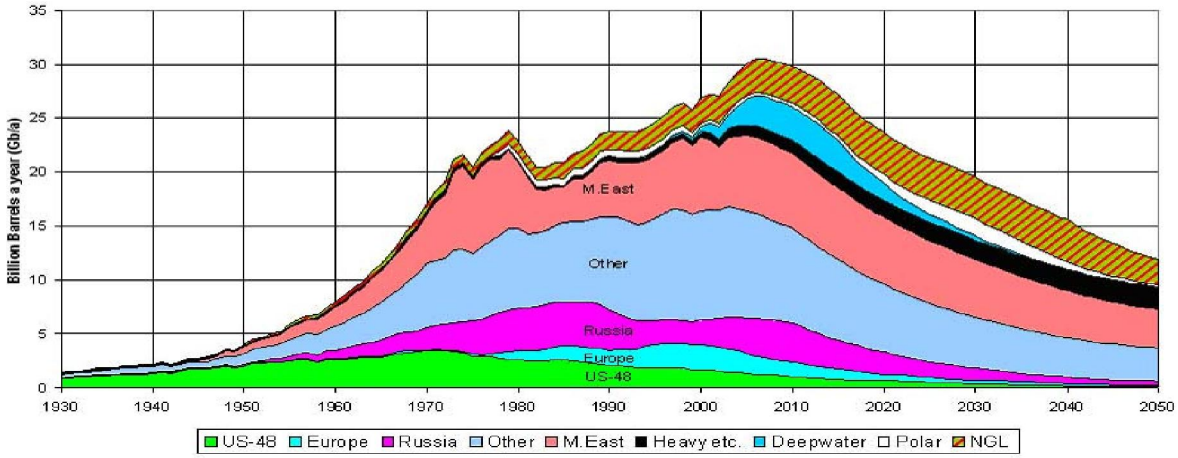

Figure (1): Regular Oil and Natural Gas Liquids [Kalogirou, 2005].

Solar energy technologies divided into two categoriesconcentrating solar power (CSP) and photovoltaic cells (PV). Both technologies use the direct normal irradiation (DNI) of the sun as a main source to generate electrical power. The main difference between photovoltaic cells and concentrating solar power plant, that the photovoltaic cells converted the sunlight directly to electrical energy by means of semiconducting materials while CSP plants, concentrate solar radiation by mirrors, which reflect the sunlight to absorber tubes.

Concentrating solar power (CSP) is considered as one of the key technologies due to its potential to meet base load applications. The IEA has set an electricity generation target of 630 GW for CSP technology by 2050. Spain has 50 CSP plants with total capacity of 2.304 GW and become the largest producer of CSP electricity. USA has 19 CSP plants with a total capacity of 1.640 GW. Countries like Algeria, Iran, Egypt, and Morocco have CSP commercial power plants integrated with natural gas combined cycles, called as integrated solar combined cycle (ISCC). But other countries having good solar resources like United Arab Emirates, Australia, China, India, Iran, Israel, Italy, Jordan, Mexico, and South Africa also have CSP programs and under construction **[Xu,2015].**

Cost of CSP plants could be reduced by the development of improved thermal energy storage (TES) fluids and improved (TES) geometry based on heat transfer modeling. Heat transfer fluid (HTF) is one of the most important components for overall performance and efficiency of CSP systems. It is necessary to minimize the cost of HTF while maximizing its performance. Besides the use of the HTF is to supply and exchange heat from solar concentrators to water in Rankin cycle. Hot HTF can be stored in a storage tank for power generation when sunlight is not available. Characteristics of a HTF include: low melting point, high boiling point and thermal stability, low vapor pressure (<1atm) at high temperature, low corrosion with metal alloys used to contain the HTF, low viscosity, high thermal conductivity, high heat capacity for energy storage, and low cost **[Vignarooban, 2015].** to improve heat transfer performance, it was necessary to increase the thermal conductivity and/or specific heat of the HTF. This could achieve by adding an appropriate amount of solid nanoparticles (NPs) having high thermal conductivity to the base fluid for use as a heat transfer fluid. Alumina is one of the most important materials that used as NPs because of its high strength and modulus, resistance to attacks from molten metals and non-oxide materials, chemical inertness in both oxidizing and reducing atmosphere up to 1,000 °C and good electrical insulation **[Tan, 2011].** The sol gel method was used to prepare Al_2O_3 NPs. Through several years of examination in the present research, eutectic salts by mixture of (NaCl- KCl- $ZnCl_2$) have been became as new generation heat transfer fluids. Eutectic salts by mixture of (NaCl- KCl- $ZnCl_2$) tested by differential scanning calorimetry (DSC) andthermogravimetric analysis (TGA) systems used for measuring heat capacity, melting temperature, heat of fusion and degree of stability.

Liddle and Sadorsky (2017) used a large panel data set of 93 countries and developed panel estimation techniques to answer the question by how much does increasing non-fossil fuels in electricity generation reduce the subsequent carbon dioxide emissions?. Where they found that a one percent increase of the non-fossil fuel electricity generation

reduced Co_2emissions per capita from electricity generation by about 0.82%. Also, they observed long-run displacement elasticity for non-fossil fuel consumption per capita of approximately 0.38. In addition to, they found also the share of non-fossil fuel for long-run displacement of electricity generation are 0.82 and with increasing one percent of non- fossil fuel used for electiricity generation reduces the Co_2emissions per capita about 0.82%, so Alternative solutions for energy utilization must be found. While, **Mundaca (2017)** illustrated that how a reduction of fossil fuel subsidies could lead to important reduction in Co_2 emissions for various groups of countries specially; Middle East, North Africa (MENA), Iran and Saudi Arabia are in advanced order of emission Co_2. He estimated that a reduction in subsidies for both gasoline and diesel by about 20 cents per liter would lead to significant decreases in Co_2 emissions, both in the MENA region and globally. In Iran and Saudi Arabia, for example, the reductions could be up to (90% and 50%), (70% and 40%) respectively of current emissions generated from diesel and gasoline consumption. Moreover, these emissions from Co_2 and other gases cause damage to the environment (environmental pollution) and climate change (warming), so researchers resorted to renewable energies especially the solar energy in the production of electricity for conservation of the environment and the atmosphere. Moreover, **Uçkun and Can (2013)** developed the mathematical model of direct steam generation (DSG) using parabolic trough collectors compared with previously published data. The results of DSG simulations showed that for lower working pressures, the overall efficiency is higher due to lower saturation temperature of the water, and consequently lower temperatures and thermal losses in the 2-phase part of the collector. On the other hand, for lower working pressures, the pressure drops are higher which can cause increase the required pumping power as a result for such a system there is a tradeoff between overall efficiency and internal energy consumption. Moreover, **Aldali and Morad (2016)** studied the thermodynamic performance of a proposed integrated solar/North Benghazi combined power plant under Libyan climatic conditions by using the PTC field with DSG. They showed that fuel saving mode; the annual saving of natural gas consumption and Co_2emission were approximately 3001.56 and 7972.25 tons, respectively. In comparison with the conventional North Benghazi combined cycle power plant, for power boosting mode, the annual solar share of electrical energy was approximately 93.33 GW hr. and the benefit/cost ratios for fuel saving and power boosting modes were 1.74 and 1.30, respectively. While, Nanofluids have been introduced as new-generation fluids able to improve energy efficiency in solar power plants where Nanofluids were presented by Choi and Eastman in (1995). They were suspensions obtained by dispersion of nanoparticles (<100 nm) in conventional fluids (water, fuel oil, ethylene-glycol, etc.). These kinds of fluids were used in heat transfer systems, heat, direct solar absorption and micro-channels, among others **[Cacua, 2017].** In addition to, **Yang et al. (2011)** showed that the dispersion of alumina (Al_2O_3) nanofluids firstly increased to a maximum and then decreased with the increase of surfactants polyacrylic acid (PAA), cetyl trimethyl ammonium bromide (CTAB), sodium dodecyl benzene sulfonate (SDBS) mass fraction. The dispersions of Al_2O_3nanofluids are improved with the increase of the mass fraction of ammonia – water base fluid. And, also, the dispersions of three kinds of nanofluids containing the mixture of α -$Al_2O_3$and PAA, γ -$Al_2O_3$and PAA, γ -$Al_2O_3$and SDBS respectively are improved by supersonic vibration period where the best dispersing performance of α-$Al_2O_3$and γ-Al_2O_3nanofluids achieved when the mass fraction of PAA is 0.3% and the supersonic vibration period is 30 min. While, **Tabesh et al. (2017)** synthesized nano-sized **γ-**Al_2O_3particles by modified sol–gel method using new precursors such as aluminum nitrate, ethylene glycol, citric acid and triethanolamine were used as an Al^{+3} source**.** They characterized **γ-**Al_2O_3particles by X-ray diffraction (XRD), scanning electron microscopy (SEM), thermo-gravimetric analysis (TGA) and infrared spectroscopy (IR). They found the average crystallite size for synthesized Al_2O_3 nanoparticles was about 6-13 nm and the maximum percentage of metal adsorption by nanostructured γ-Al_2O_3 was at pH 5. Moreover, **Li et al. (2016)** developed a HTF for CSP systems with the use of mixtures of molten chloride salts (NaCl, KCl and $ZnCl_2$) covering a working temperature ranging from 250 °C to 800 °C or above. The properties of the HTFs include; vapor pressure ≤ 1.0 atm at 800 °C, viscosity ≤0.012 Pa·s at 300 °C and ≤0.004 Pa·s at 600 °C, thermal conductivity ≥0.51 W/m·K, density ≤5400 kg/m^3, heat capacity ≥ 1.5 kJ/kg·k, and corrosion rate to a compatible metal ≤1 00μm/year. In addition to **Zhang and Li, (2017)** used various high temperature HTFs, such as, synthetic oils, various molten salts, and liquid metals to evaluate the merit of fluids regarding their transport properties. They derived a relevant equations for total entropy production as an example, the figure of merit for several HTFs used in CSP industry were compared for the goal of heat transport in the range of 50 to 600 MW. The modeling provided a fundamental approach for the comparison of various heat transport systems which might had different designs and using different HTFs/media (gas, liquid, or solid particles) in CSP systems. Moreover, **Zhao et al. (2017)** presented comparing

between supercritical carbon dioxide and the new generation molten salts (NaCl- KCl-ZnC l_2) with regard to the temperature, heat gain, the solar field efficiency and the solar exergy efficiency. They found both fluids reached to the desired temperature, heat gain under special conditions. While, **Xu et al. (2018)** studied the basic thermophysical properties of several eutectic molten salts for HTF and thermal storage media, which could work at upper limit temperatures of 850 °C. The eutectic salts were mixtures by NaCl-KCl-$ZnCl_2$, and by NaCl-KCl-$MgCl_2$, respectively. They measured the heat capacity, melting point, and heat of fusion of the eutectic salts at different temperatures by using differential scanning calorimeter (DSC) and t TGA simultaneously. They concluded the average value and the standard deviation at 95% confidence interval of these thermodynamic properties for the six eutectic mixtures.

2. Experimental Work

The alumina nanoparticles and the halide salt are prepared and developed to enhance the solar thermal performance. In the present paper the optimum thermal and thermodynamic operating conditions of parabolic trough solar power plant working with halide salts in addition to alumina NPs as a HTF were investigated. Al_2O_3 or Aluminum Oxide is the only oxide formed by the metal aluminum and occurs in nature as the minerals corundum (Al_2O_3). The definition of alumina appeared in 1754 by extracting it from natural clay using $H_2SO_4$by German scientific "Marggraf"**[Davis, 2010]**. The specific heat, thermal conductivity, heat of fusion, phase change, onset temperature and melting point of the HTF can be improved by addingAl_2O_3NPs to the base fluid (halide salt).

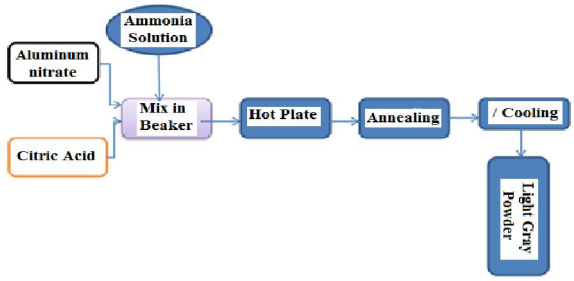

Figure (2): Flow Diagram of the Alumina Preparation Process

Figure (2) shows a schematic diagram of the alumina preparation process. Nanoparticles (Al_2O_3) were synthesized using citrate nitrate auto combustion technique "Pechini method", which defined as a process related to the sol-gel route. Aluminum nitrate (Al (N $O_3)_3$ .9 H_2 O), citric acid ($C_6H_8O_7$) and ammonia solution (NH_4OH) for pH adjustment. The nitrate and citric acid ratio was kept 1:1 (375.13:210.14 (M. W)) and pH value was adjusted at 7using droplets of ammonia under vigorous stirring the solution was heated on hotplate until a viscous gel is formed. With further heating, the gel dried and transformed to xerogel which defined as a solid formed from a gel by drying with unhindered shrinkage and fluffy black powder was obtained.

Figure (3): the Present Aluminum Nitrate, Citric Acid and Ammonia Solution Used in Alumina Preparation Process

Annealing was performed at 70 ^oC using heating and cooling rate of 10^oC/min. for 1hr. light grey powder was obtained. Figure (3) shows the typical aluminum nitrate powder, citric acid and ammonia solution, which are used in alumina preparation while figure (4) investigates the produced alumina nanoparticle powder**.**

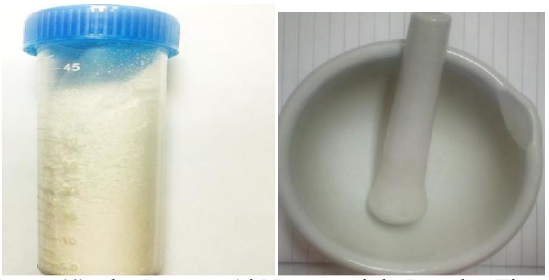

Figure (4): the Present Al Nanoparticle Powder Figure (5): The Typical Hand Mill

The pottery hand millis used to grind the powder after forming to reach the lowest possible volume of alumina grains. The powder was manually milled for at least 1 hr. until the powder was sticked onto the mill wall to ensure that the grains were reached to a very small degree. Figure (5) shows used hand mill. Also, it is used for preparing the powder before crystalline test "X-ray diffraction". The main requirements for a HTF can be summarized as follows [**Pacio et al., 2013**]: wide operation range of working temperature, regarding physical properties, a large thermal conductivity is desired for efficient heat transfer, a low viscosity is beneficial to pressure drop and pumping power and a large heat capacity and

operational aspects such as safety and corrosion behavior have a major role, less expensive and chemical stability. In that context, a novel eutectic salt of (NaCl–KCl–Zn Cl_2) was proposed as a new generation high-temperature because of the wide operating range of the working temperatures. Using salt as the receiver HTF is also appealing because the same fluid can be used as the storage medium, eliminating the need for an intermediate heat exchanger between the receiver and thermal storage. The heat transfer performance of fluid is one of the main influencing factors of the CSP thermal performances. The advantages of eutectic salt (NaCl – KCl –Zn Cl_2) are low vapor pressure, high boiling point, and controllable low corrosion rate to high temperature metals under certain circumstances have been observed for theses salts **[Vignarooban et al., 2015]**. Very importantly, these chloride salts have relatively low cost and are abundant in nature. So this salt in the present work will be studied. The three ternary eutectic salt can satisfy melting point criterion T_{eu1} =229°C at (NaCl-KCl- Zn Cl_2) mole fraction of (8.1%-31.3%-60.6%), T_{eu2} =213°C at (NaCl-KCl- $ZnCl_2$) mole fraction of (18.6%-21.9%-59.5%) and T_{eu3} =204°C with mole fractions of (13.4%-33.7%-52.9%) which uses in studying the compositions of the three salts and mechanical properties, **[Li et al, 2016].** Sodium chloride, potassium chloride and zinc chloride were procured from lobal chemie. The following consequent steps represent the detailed experimental procedures of the ternary eutectic salt**.** Initially, 200 mg of eutectic (NaCl- KCl- $ZnCl_2$) in solid state (13.4-33.7-52.9) by wt.% was measured on a micro balance (Mettlar, Model AE420). The mixture is then dissolved with 20 ml of distilled water and stirred for (200-250) min. in magnetic stirrer (MS400 Hotplate Magnetic Stirrer, Bante Instruments Co.) to ensure a good dispersion of the mixture and to minimize potential agglomeration of particles. After stirring, the solution is then heated for 4 hr. in a mufflefurnace to obtain the dehydrated salt. To remove any absorbed moisture, the sample was kept at 100 °C for 30 min. on a hot plate before each experiment. Figure (6) shows a schematic diagram of the eutectic ternary salts preparation.

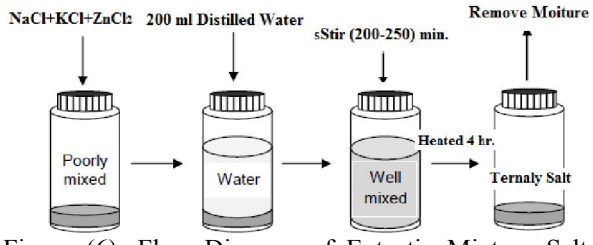

Figure (6): Flow Diagram of Eutectic Mixture Salt Preparation

The same procedure for Halide Salt was followed to prepare the nanofluids with different concentrations 0.5, 1.0, 1.5 and 2.0 wt.% of nanoparticles. Figure (7) investigates the flow diagram of nanofluid.

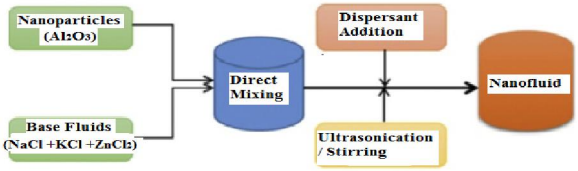

Figure (7): The Schematic Diagram of Nanofluid

All the materials used in the present work were subjected to dehydration in order to remove all the water bubbles. After this operation, the DSC analysis immediately is used to avoid any possible negative effect of the water.

3. Operating Parameters

The ranges of the operating parameters applied in the present investigation are following given in:

- The Bragg diffracted angle (2θ) is varying from 15 to 80 degree.
- The peak intensity of Al_2O_3 is varying from 0 to 60 A.U.
- The supply temperature is varying from 0 to 850 °C.
- The range of specific heat capacity is from 0 to 5 J/g °C.
- The concentration by weight of NPs is varying from 0 to 2.0 wt.%.
- The sample weight percent is varying from 0 to 100 %.

4. Specimen Preparation Instruments

In the present paper, the base HTF and nanofluid specimens were prepared and developed by preparation equipment such as **MS400 magnetic stirrer** used for preparing the specimens via blinding the HTF components (NaCl- KCl-$ZnCl_2$) and/or with (Al_2O_3) at 1000-1250 rpm and working as a heater to remove the moisture from the sample before carrying out the experiment.

Moreover the present **muffle furnace** used for drying the samples at temperature reaches to 200 °C after stirring process. The present furnace consists of temperature controller, K-type thermocouple, electric heater elements, housing and safe door while the present (DTC303) temperature controller used for reach the required temperature in a minimum possible time with keeping the desired temperature. The present body of muffle furnace constructed with powder-coated steel body, ceramic fiber insulation

where ceramic fiber exposed for heating interior from two sides of electric heater elements.

5. Measuring Instruments

In the presented paper, the considered parameters that affecting the performance such as **(**alumina structure**,** alumina concentration, supplying temperature, melting point of HTF, onset temperature, phase change temperature, specific heat and heat of fusion) are examined by measuring instruments such as **the typical (AE420) microbalance** used to weigh the samples with gram and milligram. The microbalance provides with the sliding glass doors to ensure measurement accuracy. The **present thermocouple** applied in muffle furnace to determine the specimen temperature. The temperatures were measured by using (K-type) thermocouple (with accuracy of ± 0.2 °C and range of temperature between −270 to 1260 °C). In addition to **X-ray Diffractometer (XRD)** enables crystalline phases to be identified, quantified, and their crystal structure determined. It is worth to mention that, X-ray diffraction (XRD) is the method of choice for extracting structural information from virtually any type of sample, regardless of shape, size or composition, under ambient or non-ambient conditions where the output photograph shows how the intensity of diffracted radiation (**I**) varies with the angle of diffraction (2**θ**), consists of peak positions, intensities, oscillations and other shapes, which are characteristic for the present sample. Using this data, one can deduce the sample properties in detail. Moreover **High Resolution Transmission Electron Microscopy Quanta 250 (HRTEM)** has the ability to show images of crystalline structures of samples at the atomic level and is used to study the properties of crystalline materials at the nanoscale level, determines the average size of nanopowder and shows the electron diffraction image. The highest accuracy of HRTEM is 0.08 nm. While, **Differential Scanning Calorimetry Q2000 (DSC)** is used for measuring heat capacity, melting temperature, onset temperature, phase change temperature, offset temperature and heatof fusion. The present DSC has Platinum software, which permits automatic scheduling of tests designed to keep it consistently in top operating condition. The present DSC consist of photocalorimeter, pressure DSC, and the cooling devices. Finally, **Thermogravimetric Analysis Q500 (TGA)** is a thermal analysis method that monitors changes in the physical and chemical properties of the material. The process is performed during the temperature increase where the thermal weight analysis device continuously weights the sample while heating to high temperature range about 1000-2000°C. As the temperature increases, the components of the sample decompose and measured at the same time the percentage change in the sample weight. The present TGA consist of the furnace, the key element of present thermogravimetric analysis (Q500), the heart of a Q500 TGA is the accurate and reliable vertical thermobalance housed in a temperature-compensated environment and a single thermocouple positioned immediately adjacent to the sample.

6. Discussion of the Results

The current work concentrates on adding homogeneously dispersed alumina particles into eutectic ternary halide salt. So, the thermal properties improved and led to high a heat transfer rate within solar system. Based on these results, it could be demonstrated that alumina was an effective additive to enhance thermal properties of chloride salts.

6.1 The Definition of the Most Effective Parameters that Affect the Present System Performance

In this section, it will present the definitions of the main effective parameters that affect the performance of the present modified heat transfer fluid with nanoparticles. These are:

1- The Bragg diffracted angle is defined as:

$$\mathbf{2\sin\theta(degree)} = \frac{\mathbf{n\times\lambda(meter)}}{\mathbf{d(meter)}} \quad \text{..... (1)}$$

Where **n** is an integer, **λ** is the wavelength of a beam of x-rays incident on a crystal with lattice planes separated by distance **d**, and **θ** is the Bragg angle

2- The specific heat capacity "Cp" (J/g.°C)is defined as:

$$\text{Cp (J/g.}^{o}\text{C)} = \frac{\mathbf{Q(joule)}}{\mathbf{m(gram)\times\Delta T(degreecelsius)}} \quad \text{..... (2)}$$

Where **Q** is a heat added within DSC analysis to specimen mass **m**, **Δ T** is the temperature change during the process.

3- The weight percent "wt%" is defined as:

$$\text{wt\%} = \frac{\mathbf{\Delta w\ (grame)}}{\mathbf{w_{tot.}\ (grame)}}\mathbf{X100} \quad \text{..... (3)}$$

Where **Δw** is the weight changed during temperature raise in TGA analysis, $\mathbf{w_{tot.}}$ is the total weight of sample in crucible.

4- The heat of fusion of specimen "H_f" is determined as:

The area covered by the Cp−T curve under the peak that is due to melting process.

$$H_f\,(kJ/kg) = \int_{T_i}^{T_f}\left[\mathbf{C_p(T) - C_{p,base}}\right]\mathbf{dT} \quad \text{..... (4)}$$

Where $\mathbf{T_i}$ and $\mathbf{T_f}$ are the initial and final temperatures of the peak, **Cp, base** is the baseline value.

5- The onset temperature (T_{on}) of specimen is determined by the inter section of the extrapolated baseline and the tangent line drawn at the inflection point on the lower temperature side of the fusion peak and is considered the beginning of melting.

6- The offset-temperature (T_{off}) is the designed intersection point of the extrapolated baseline and the inflectional tangent at the beginning of the melting or crystallization peak. The baseline and the inflectional tangent are determined from the temperature-dependent heat flow signal.

7- The melting temperature of specimen (T_m) is the point that divides the area under the curve into two equal parts and is considered the complete melting point.

8- The phase change temperature (T_{pc}) is defined as the different between the onset temperature and the end of the transition (offset temperature).

9- Peak intensity (I) which Refers to the strengh of X-rays scattered by the sample at different angles between the beam incident on the sample and beam scattered by the sample.

6.2 Verification between the Present Experimental Prepared Al_2O_3 NPs with the Reference Al_2O_3 NPs

Alumina (Al_2O_3) has been synthesized through Pechini method, related to sol gel method. The calcined products were characterized using XRDand HRTEM. The phase γ-Al_2O_3 was formed in the temperature range from (600 - 800)°C as deduced from the XRD patterns with (h k l) directionsof cubic crystal structure. The variations between Bragg angle (2θ) and peak intensity with coordinate direction (h k l) is shown in figure (8). the figure states at the different Brag angle, the peak is formed. This mean that the phase structure is created. To verify that the specimen is alumina with phase structure gamma. A comparison was made between the present experimental prepared sample analysis and the preceding of the corresponding previous work of **Eid et al. (2019)**, for a nearly the same working conditions, as shown in figure (9). The present figure demonstrates the variation between Bragg angle and peak intensity. The variation of both results **Eid et al (2019)** and the present work are similar within the range of Bragg angle (2θ) of 15 to 80 degree. But the peaks don't identical relatively because of lattice strain. The agreement of the present experimental analysis with that of **Eid et al. (2019)** is fairly good through the plane of atoms (h k l). The avarage size of Al_2O_3 nanoparticles was measured by HRTEM as shown in figure (10).

It was observed that the average grainsize of Al_2O_3 NPs is 26.87 nm where the change in grain size is observed with enlargement of the diffraction peaks.

6.3 Influence of Temperature of Pure Halide Salt and Nanofluid with Different Concentrations of NPs

The following section presents the effect of temperature of halide salt without or with nanoparticles on its thermal properties (the specific heat, phase change temperature, the heat of fusion, the melting point, and the onset temperatures). TGA and DSC used for measuring the upper temperature limit of halide salt and nanofluid (thermal stability) and their thermal properties respectively.

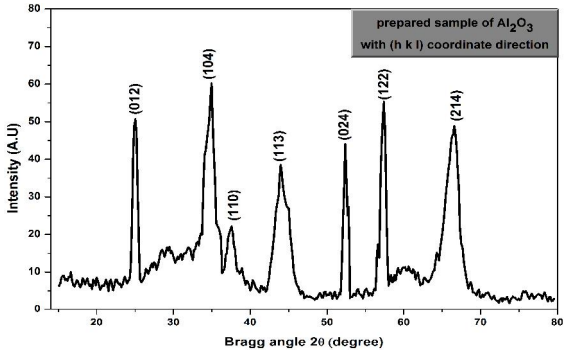

Figure (8): XRD Analysis Curve for Prepared Spacimen

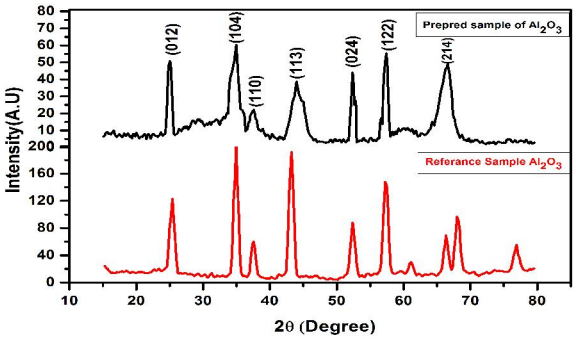

Figure (9): Comparison between Atoms Plane Values (h k l) of Prepared Al_2O_3 NPs and Reference Al_2O_3 of Eid et al. (2019).

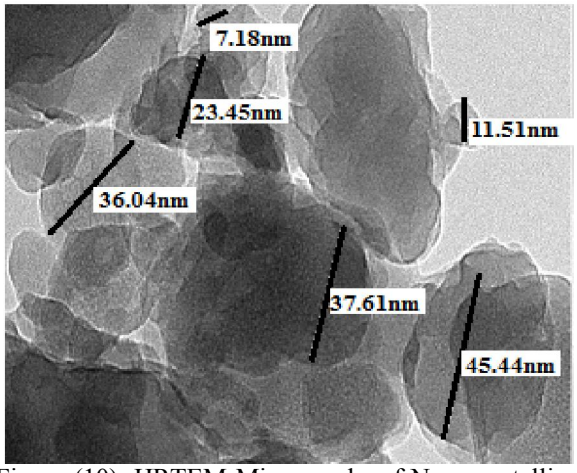

Figure (10): HRTEM Micrographs of Nanocrystalline Al_2O_3 Powders at Different Size.

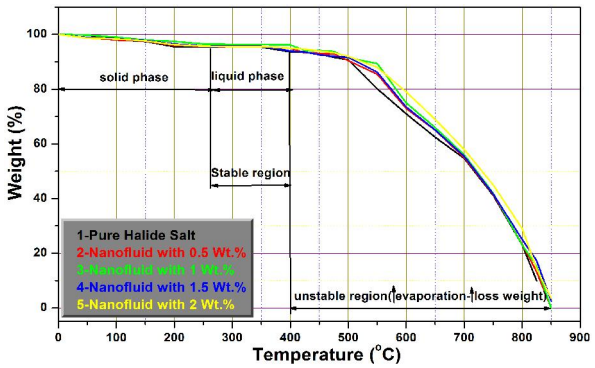

Figure (11): Variation of Temperatures at Different Concentrations of Al_2O_3 with Weight (%) of Specimens.

Figure (11) presents the TGA curve, which indicates the weight changes in the sample material as a function of temperature. The figure shows that, the weight percent of sample is affected by the increase of the specimen temperature. The variation of sample weight percent is varying from 100 to 0 % with the variation of sample temperature from 0 to 850 °C respectively. The experiment was performed at different values of nanoparticles as 0, 0.5, 1.0, 1.5 and 2.0 wt.% from total sample mass. The following observations can be concluded by inspection of the representing curves. As the temperature of salt (sample) increases, the evaporation rate becomes larger and consequently the heat of evaporation effect will be much stronger; the measured data is no longer valid (i.e. the weight percent of salt sample collapses with increasing temperature). In the solid phase, the wt.% decreased by 5% with increasing the temperature while the wt.% is independent with the temperature in liquid phase. When the concentration of Al_2O_3 NPs increases, the stability of the nanofluid increases at 400 °C, the nanofluid evaporates more, the loss weight increases; the nanofluid starts to enter the unstable region until it reaches to Collapse at about 850 °C.

6.4 Differential Scanning Calorimeter (DSC) Analyzes for Different Concentrations of Al2O3 Nanoparticles within Halide Salt.

It is worth to mention that the following section will present the different concentrations of Al_2O_3 nanoparticles in halide salt by DSC analysis that will appear in figure (12) through figure (16).

It can be noticed that a sufficient number of measurements are necessary in order to reduce the random error thus; three readings were taken for the present sample of halide salt to eliminate it. Figure (12) presents the variation of temperature (°C) with the specific heat "Cp"(J/g.°C) for pure cloride salt with a trial of measurements under the following conditions:

- The supply temperature of the sample varies througth the range of (50 to 400)°C.
- The feed concentration of NPs witin halide salt is 0.00 wt.% (pure salt).

Under this conditions it can conclude the following detailed values were obtained by the measured DSC curve (inspection of figure (12)):

- The avarage onset temperature is 199.29 °C.
- The avarage melting temperature is 226.676 °C.
- The avarage offset temperatureis 256 °C.
- The peakat about 199.29 -256 °C was formed by the solid-liquid phase change temperature.
- The avarage specific heat capacityis 1.0416 (J/g.°C).
- The avarage heat fusionat is 69.34 (kJ/kg).

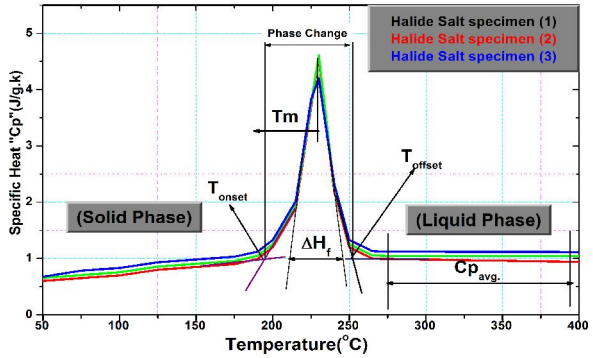

Figure (12): Differential Scanning Calorimeter Analyzes for Pure Chloride Salts (Halide Salt).

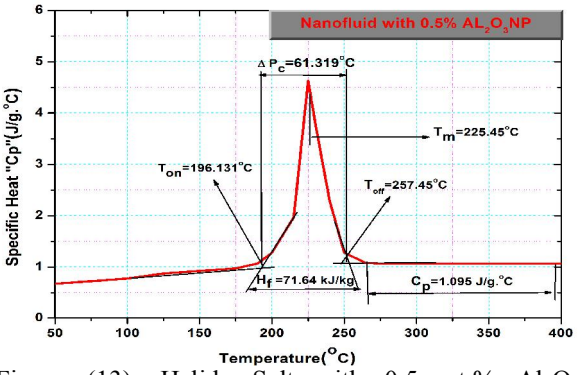

Figure (13): Halide Salt with 0.5 wt.% Al_2O_3 Nanoparticles Analysis by DSC.

The negative heat flow (positive heat capacity) implied that heat was absorbed by the sample in the melting process. The sharp single peaks signified the solid-liquid phase transition of the sample. A general trend seen from the curves for the present chloride salts in NaCl-KCl-$ZnCl_2$ system indicates a very weak temperature-dependency for the heat capacity especially in liquid phase. On the other hand, the

present halide salt presents a strong temperature-dependence for the heat capacity in solid phase.

Figure (13) presents the development of the feed temperature (^{o}C) and the improved specific heat capacity "Cp"(J/g.^{o}C) for cloride salts (NaCl-KCl-$ZnCl_2$) withnanoparticles. The supply temperature of the speciemen is varying from 50 to 400 ^{o}C. The feed concentration of NPs witin the present halide salt is about 0.5 wt.%. The present obtained results from DSC curve have promising values than the corresponding one, presented in figure (12), due to Brownian motion of nanoparticles which defined as a random movement of microscopic particles suspended in liquids or gases resulting from the impact of molecules of the surrounding medium and nature of heat transport in nanoparticles and nanoparticle clustering **[Dudda and Shin, (2013)].**

Figure (13) demonstrates that the addition of 0.5 wt.% Al_2O_3 nanoparticles significantly increases the phase change temperature different, the heat fusion and the specific heat capacity of halide salt by 8.13%, 3.32% and 5.13% respectively on the other hand the onset temperature, the offset temperature and the melting temperature decreased by 1.585%, 0.566% and 0.54% respectively.

It is a geometric logic that the increase of nanoparticles in the HTF improves its thermal properties as a significant increase in the specific heat of the liquid has been observed. this results is reflected positively on the performance of the solar system.

Inspection of figure (14), it was concluded that the specific heat increases to 14.8% with respect to 0.0 wt.% NPs. the heat fusion increased approximately by 10.93% through adding alumina nanoparticles with weight concentration of 1.0 %, compared with the heat fusion of pure salt. An enhancement of 23.15% in the phase change temperature was observed by adding Al_2O_3 NPs with weight concentration of 1.0 %. the offset temperature value increases by 2.96% than the corresponding onefor pure salt.

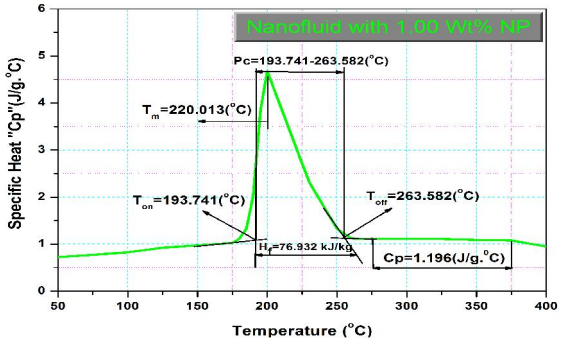

Figure (14): Effect of 1.00 wt% Al_2O_3 Nanoparticles on Halide Salt.

The total decrease in onset temperature due to concentration by weight increase from 0 to 1.0% is 2.78%. according to increasing the concentration of NPs from 0.5-1.0 wt.%, this causes a decrease in melting temperature with a mean value 2.94 %.

Furthermore, this concentration of nanoparticles in halide salt is the better for the rest of the concentrations.

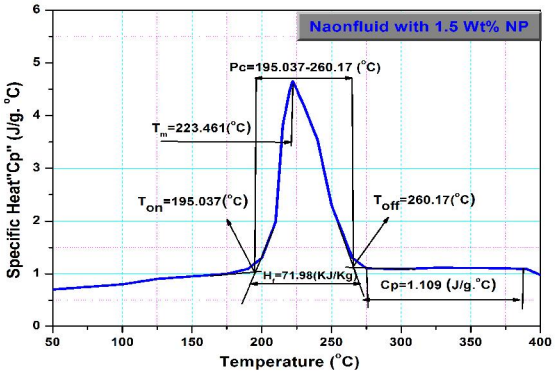

Figure (15): Differential Scanning Calorimeter Analyzes for Nanofluid with 1.5 wt% NPs.

Figure (15) presents a detailed examination of the effect of the concentration of Al_2O_3 nanoparticles on the (onset, offset and melting Temperature- heat fusion- phase change- specific heat) of ternary eutectic salt. this data will be shown in the following table.

Table (1): Enhancement of Thermal Proparties of Halide Salt at 1.5wt.% NPs

Thermal proparties	T_{on}	T_{off}	T_m	ΔP_c	H_f	Cp
Enhancement of 1.5wt.% compared with 0.0wt.%	**↓2.13%**	**↑1.63%**	**↓1.42%**	**↑14.85%**	**↑3.81%**	**↑6.47%**

The present table indicates that the addition of nanoparticles to base salt by 1.5 wt.% increased the offset temperature, phase change temperature, the heat fusion and specific heat capacity while decreased the onset temperature and melting temperature compared to the pure salt (0.0 wt%). Comparing this results of 1.5 wt% of nanoparticles with 1.0 wt.% NPs. The results were dissimilar to the expectations. When increasing the nanoparticles in pure salt, the thermal properties of the substance are expected to improve, but the results show the opposite because of the agglomeration of nanoparticles where appears to be greater and the formed clusters become huge and increasingly inter-connected as the concentration of

Al_2O_3 nanoparticles in ternary is increased, as indicated by the results **[Ho and pan, (2014)].**

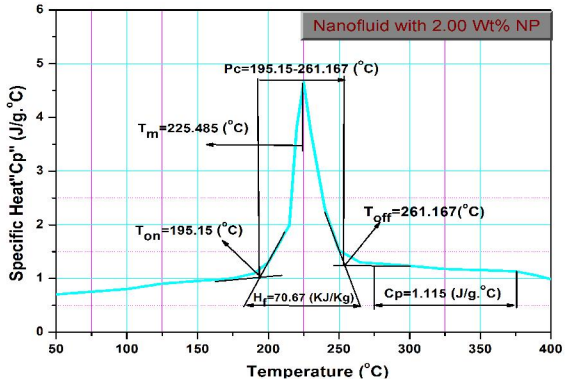

Figure (16): Nanofluid with 2.0 wt.% Al_2O_3 Nanoparticles Analysis by DSC.

Figure (16) presents the effect of 2.0 wt.% nanoparticles on ternary eutectic salt. As shown from the present figure, one can conclude the following:

- The value of The specific heat, heat fusion, offset temperature and phase change increases by 7.04%, 1.91%, 2.02% and 6.41%, respectively, with the increase of NPs by 2.0 wt.%.
- As the addition of nanoparticles to base salt increases by 2.0 wt.%, the melting temperature and onset temperature decreases by 0.53% and 2.08% respectively.
- The specific heat, heat fusion, offset temperature and phase change slightly increase with increases by 2.0 wt.% concentration of NPs which confirm the preceding results shown in figure (15).

7. Conclusions

In the present work, developing the performance of nanofluid based solar power system is experimentally investigated. From the previously presented results, the following main are extracted:

Adding Al_2O_3nanoparticles from 0.0 wt.% to 2.0 wt.% to unmodified base salt solution leads to an increase in the specific heat capacity, heat of fusion, phase change temperatures, stability percentage respectively. However, both melting point and onset temperatures decrease.

The following main conclusions extracted from adding the Al_2O_3 NPs from 0.0 wt.% to 1.0 wt.%,:

a- The maximum enhancement is occurred for the thermal properties of nanofluid compared to the unmodified base salt solution.

b- A clear reduction in weight loss up to 12.5% (i.e. which means rising of the stability of HTF by evaporation.

c- The onset temperature reduced by 2.8% (i.e. 5.5 °C) and the melting temperature lowered by 2.9% (i.e. 6.5 °C) rather than base salt temperature.

d- Specific heat capacity, heat of fusion and phase change of the salt mixture increased by 14%, 10.9% and 23.2% respectively.

While the following main conclusions extracted from adding the Al_2O_3 NPs from higher than 1.0 wt.%:

a- There is an insignificant change in thermal properties of nanofluid with the range of Al_2O_3 NPs from 1.5 wt.% to 2.0 wt.%.

b- The results revealed that the agglomeration of nanoparticles in halide salt becomes stronger and the enhancement of specific heat capacity may even become negative as the concentration of the nanoparticles increases above 1.0 wt.%.

Finally, The enhanced specific heat capacity of the nanofluids can significantly reduce the required amount of thermal energy storage media, i.e the size of thermal transport system in concentrated solar power plants with a consequent reduction in the cost of electricity.

Nomenclature

I=Intensity (A.U)

θ=Bragg Diffracted Angle (Degree)

Greeks

α=Alpha

γ=Gamma

Abbreviations

$SO_{2=}$ Sulfur Dioxide

SO_3= Sulfur Trioxide

H_2SO_4= Sulfuric Acid

CSP= Concentrating Solar Power

PV= Photovoltaic

DNI= Direct Normal Irradiation

IEA= International Energy Agency

ISCC= Integrated Solar Combined Cycle

TES= Thermal Energy Storage

HTF= Heat Transfer Fluid

MENA= Middle East, North Africa

DSG= Direct Steam Generation

PTC= Parabolic Trough Collector

Al_2O_3= Alumina

PAA= Poly Acrylic Acid

CTAB= Cetyl Trimethyl Ammonium Bromide

SDBS= Sodium Dodecyl Benzene Sulfonate

XRD= X-ray diffraction

SEM= Scanning Electron Microscopy

TGA= Thermo-Gravimetric Analysis

IR= Infrared Spectroscopy

DSC= Differential Scanning Calorimeter

NP= Nanopartical

HRTEM= High Resolution Transmission Electron Microscopy

References

1. Kalogirou A.S., (2005), "Seawater Desalination Using Renewable Energy Sources." Progress in Energy and Combustion Science 31, PP. 242-281.
2. Liddle B., and Sadorsky P., (2017), "How much does Increasing non-Fossil fuels in Electricity Generation Reduce Carbon Dioxide Emissions?" Applied Energy 197, PP. 212-221.- Uçkun C. and Can S., (2013)" Modeling and Simulations of Direct Steam Generation in Concentrating Solar Power Plants Using Parabolic Trough Collectors", M.Sc. thesis, Middle East Technical University.
3. Vignarooban K., Xu X., Arvay A., Hsu K., and Kannan A.M., (2015), "Heat Transfer Fluids for Concentrating Solar Power Systems – A review." Applied Energy 146, PP.383–396.
4. Xu B., Li P., and Chan C., (2015), "Application of Phase Change Materials for Thermal Energy Storage in Concentrated Solar Thermal Power Plants: A review to Recent Developments." Applied Energy 160, PP.286–307.
5. Aldali Y., and Morad K. (2016), "Numerical Simulation of the Integrated Solar/North Benghazi combined power plant." Applied Thermal Engineering 108, PP. 785–792.
6. Cacua K., Sierra R.B., Herrera B., Chejne F., and Pabón E., (2017), "Influence of Different Parameters and their Coupled Effects on the Stability of Alumina Nanofluids by a fractional Factorial Design Approach." Advanced Powder Technology 28, PP. 2581–2588.
7. Davis K., (2010), "Material Review: Alumina (Al_2O_3)" School of Doctoral Studies European Union Journal, (2).
8. Dudda B., and Shin D., (2013) "Effect of Nanoparticle Dispersion on Specific Heat Capacity of a binary Nitrate Salt Eutectic for Concentrated Solar Power Applications" International Journal of Thermal Sciences 69, PP.37-42.
9. Eid E. A., El-Basaty A. B., Deghady A. M., Kaytbay S. and Nassar A., (2019) "Influence of Nano-Metric Al_2O_3 Particles Addition on Thermal Behavior, Microstructural and Tensile Characteristics of Hypoeutectic Sn-0.5 Zn-0.3 Cu Pb-Free Solder Alloy" Journal of Materials Science.
10. Ho M. and pan C., (2014) "Optimal Concentration of Alumina Nanoparticles in Molten Hitec Salt to Maximize its Specific Heat Capacity" International Journal of Heat and Mass Transfer 70, PP.174–184.
11. Li P., Chan C., Hao Q., Deymier P., Muralidharan K., Gervasio D., Momayez M., Jeter S., Teja A., and Kannan A., (2016), "Halide and Oxy-Halide Eutectic Systems for High Performance High Temperature Heat Transfer Fluids." SunShot Concentrating Solar Power Program Review, PP. 85-86.
12. Mundaca G., (2017)," How much can CO_2 Emissions be Reduced if Fossil Fuel Subsidies are Removed?" Energy Economics 64, PP. 91-104.
13. Pacio J., and Wetzel T., (2013), "Assessment of Liquid Metal Technology Status and Research Paths for their Use as Efficient Heat Transfer Fluids in Solar Central Receiver Systems" Solar Energy 93, PP. 11–22.
14. Tabesh S., Davar F., and Loghman-Estarki M.R., (2017), "Preparation of γ-Al_2O_3 Nanoparticles Using Modified Sol-Gel Method and its Use for the Adsorption of Lead and Cadmium Ions." journal of alloys and compounds.
15. Tan H.b., and Guo C.S., (2011)," Preparation of Long Alumina Fibers by Sol-Gel Method -Using Malic Acid." Transactions of Nonferrous Metals Society of China 21, PP. 1563-1567.
16. Xu X., Dehghani G., Ning J., and Li P., (2018), "Basic Properties of Eutectic Chloride Salts NaCl-KCl-$ZnCl_2$ and NaCl-KCl-$MgCl_2$ as HTFs and Thermal Sorage Media Measured Using Simultaneous DSC-TGA" Solar Energy 162, PP.431–441.
17. Yang L., Du K., Zhang X.S., and Cheng B., (2011), "Preparation and Stability of Al_2O_3 Nano-Particle Suspension of Ammoniae Water Solution" Applied Thermal Engineering 31, PP.3643-3647.
18. Zhang Y., and Li P., (2017), "Minimum System Entropy Production as the FOM of High Temperature Heat Transfer Fluids for CSP Systems." Solar Energy 124, PP.342-353.
19. Zhao Y., Li P., and Jin H., (2017), "Heat Transfer Performance Comparisons Of Supercritical Carbon Dioxide And Nacl–Kcl–$Zncl_2$ Eutectic Salts For Solar S-Co_2 Brayton Cycle." Energy Procedia 142, PP. 680-687.

4/21/2019